A Permanent-magnet Double-stator Integrated-starter-generator for Hybrid Electric Vehicles

Shuangxia Niu*, K.T. Chau*, Senior Member, IEEE, and J.Z. Jiang**
* Department of Electrical and Electronic Engineering, the University of Hong Kong, Hong Kong, China.
Email: sxniu@eee.hku.hk
** College of Mechatronics Engineering and Automation, Shanghai University, Shanghai, China.
Email: jzhjiang@mail.shu.edu.cn

Abstract—**This paper presents a new permanent magnet double-stator integrated-starter-generator (ISG) for hybrid electric vehicles (HEVs). Compared with conventional PM electric machines, it has the advantage that currents of both the inner and outer stators produce electromagnetic torque and two air-gaps can deliver the output torque, thus improving the torque density and providing a high starting torque for cold cranking. Because of the nature of double-stator windings, the machine can flexibly change their connections, hence providing a constant output voltage over a wide speed range for battery charging. By using time-stepping finite element method (TS-FEM), the steady-state and dynamic performance of the machine is analyzed. Hence, due to the high starting torque and good controllability, this proposed ISG is desirable for HEVs application. A three-phase 22-pole 2 kW prototype is designed and built for experimentation verification.**

Keywords — **Double-stator machine; Permanent-magnet machine; Integrated starter-generator; Time-stepping finite element method**

I. INTRODUCTION

Faced with the ever rising global oil price and a continuous deterioration of ecological environment, hybrid electric vehicles (HEVs) technology attracts much more attention than ever before. Integrated-starter-generator (ISG) is one kind of attracting technique used in HEVs applications, which combines the functions of starting engine and generation electric power by one electric machine, hence owes the virtues of energy economizing and high efficiency [1-3]. However, ISG requires many rigorous specifications, such as a very high starting torque for cold cranking, and a constant output voltage over a very wide speed range for battery charging.[4],[5]. It is difficult for conventional electric machines to meet the requirements simultaneously.

Because of high efficiency and high power density, permanent-magnet (PM) machines are proved to be a competitive candidate for ISG system of EVs applciations [6-9]. However, due to the absence of flux control, a highly fluctuating output voltage under varying speeds is usually caused. Recently, the concept of a flexible winding control in double-stator PM machine has been introduced for wind power generation application [10]. This method can generate a constant output voltage under a wide wind speed range. In this paper, this idea is further extended to the ISG in HEVs to obtain a constant battery charging voltage within a wide speed range in generation mode. A PM double-stator integrated-starter-generator for HEVs application is newly proposed. The unique machine configuration and flexible double-stator winding connections are introduced in detail. The steady state and transient performance of the machine is analyzed by time-stepping finite element methods (TS-FEM). Simulation and experimental results verify its suitability for HEV propulsion.

II. DESIGN AND ANALYSIS OF THE PROPOSED ISG

A. Machine Configuration

For conventional starter-generator in automobiles, the starter motor and generator are separately belt-driven. Due to that the machine serves as starter only during the time of engine starting, which is less than 1% of the total driving time. In order to avoid the heavy weight and bulky size of system and fully utilize the function of machine, direct driven ISG is proposed and it is mounted with crankshaft directly and placed between ICE and clutch. For the purpose of eliminate the complicated mechanical connection with clutch, a novel ISG system is proposed in this paper. Fig. 1 shows the structure of the proposed automotive electrical systems of HEV, in which a double-stator PM brushless machine serves as the ISG placed on the left side of clutch.

Fig. 2 shows the structure of the double-stator permanent magnet machine. There are 24 slots wounded with 3-phase windings in the concentric outer and inner stator. 22 pieces of PMs (N-poles are shaded whereas S-poles are unshaded) are separately mounted on the inside and outside surfaces of the rotor. Two winding arrangements method, 3-phase single-layer and 3-phase double-layer, can be applied in both the inner and outer stators, as shown in Fig. 3. At any position, two phases are conducting whereas the third phase is in the nonconducting state. Each phase winding conducts for 120° and then in the nonconducting state for 60°.

There are some distinct merits for this proposed permanent magnet double-stator ISG. First of all, the arrangement of fractional number of slots per pole per phase (namely, the slot-pitch is 11/12 of the pole-pitch) can significantly reduce the cogging torque that usually occurs in other PM machines. Additionally, the structure of cup-shaped rotor and two concentric stators can effectively improve the torque density, hence improving the starting torque. Finally, the connection of two stator windings can provide independent and flexible control, so

978-1-4244-1849-7/08/$25.00©2008 IEEE

that the output voltage can be kept constant, hence avoiding the over voltage in the generation mode.

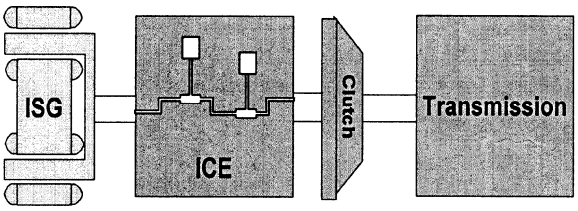

Figure 1. Proposed ISG system

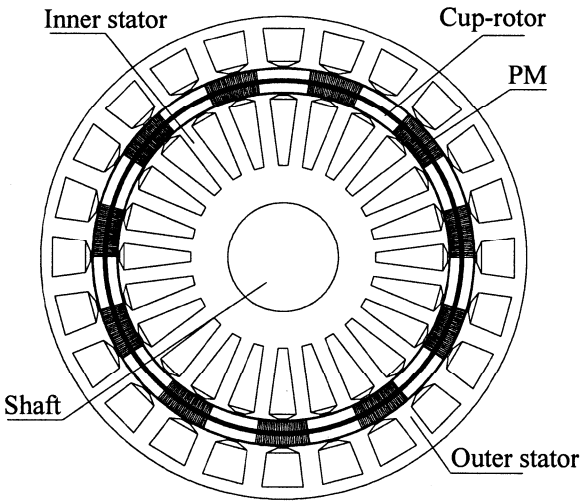

Figure 2. Configuration of the permanent magnet double-stator ISG.

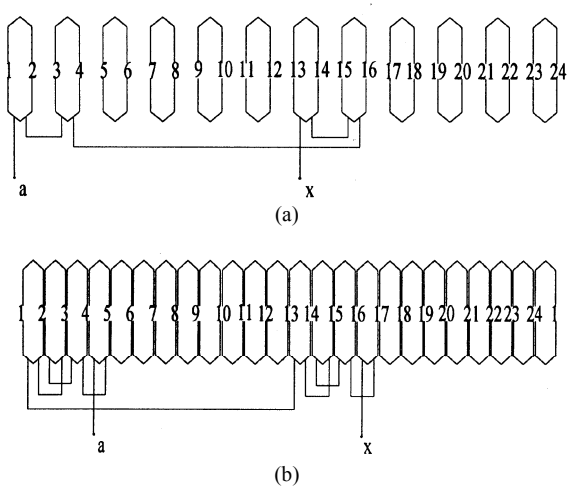

Figure 3. Winding arrangement diagram (one phase is connected). (a) Single-layer winding. (b) Double-layer winding.

B. *Equivalent Magnetic Circuit and analysis*

Double-stator ISG can be considered as combining two machines together, one is a single-stator inner-rotor machine, and the other is a single-stator outer-rotor machine. These two machines have the same armature diameter and two rotors are combined with a rotor iron core, hence reducing the yoke of rotors. This structure improves the utilization of space and improves the torque density. The main magnetic circuits of double-stator ISG, traditional single-stator inner rotor PM machine and traditional single-stator outer rotor PM machine are shown in Fig. 4. R_1 is the magnetic reluctivity of outer stator iron core, R_1' is the magnetic reluctivity of inner stator iron core, R_2 is the magnetic reluctivity of the outer airgap and PM, R_2' is the magnetic reluctivity of the inner airgap and PM, R_3 is the magnetic reluctivity of the radial rotor iron core, R_4 is the magnetic reluctivity of the rotor yoke in single-stator machine, F_1 and F_2 are the PM MMF. It can be shown that the double-stator configuration with the cup-shaped rotor can effectively shorten the magnetic circuit length and hence improve the utilization of active material.

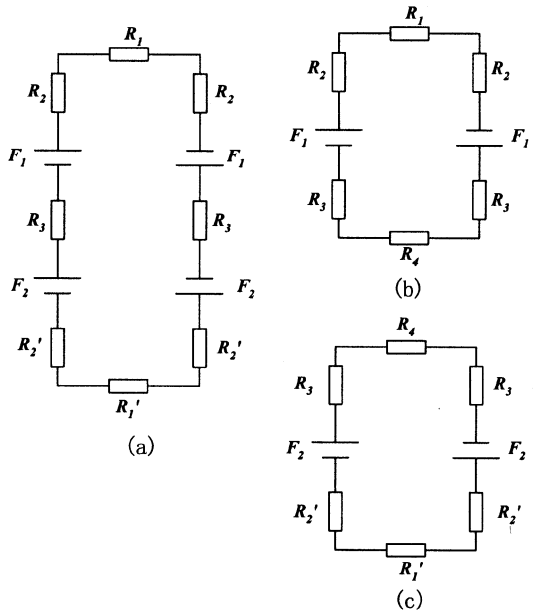

Figure 4. The comparison of main magnetic circuit. (a) Double-stator machine. (b) Traditional single-stator inner rotor PM machine. (c) Traditional single-stator outer rotor PM machine.

C. *Principle of Operation*

Due to the double-stator structure, the outer stator provides 6 terminals from these 3-phase windings, and correspondingly, 6 terminals are provided in the inner stator. Owing to the special double-stator structure of machine, the two sets of 3-phase stator windings can be flexibly connected over a wide speed range for battery charging. The connection modes are shown in Fig. 5 and the corresponding vector diagrams are illustrated in Fig. 6. $\dot{E}_{A+a}$ is the electric potential vector of one phase in the mode of the same phases in series, E_{A-b} is the electric potential vector of one phase in the mode of adjacent anti-phases in series, and E_{A+b} is the electric potential vector of one phase in the mode of adjacent phases in series. Under the same speed ω, the relationship of various generated EMF with different connection mode are listed in Table I. Based on the vector diagrams shown in Fig. 6, it can be found that $E_{A+a} \approx 2E_a$, $E_{A-b} \approx 2/\sqrt{3}E_a$,

$E_{A+b} \approx E_a$, which demonstrates that the generated output voltage can be discretely tuned. According to different speed range, we can choose corresponding connection mode to avoid the over voltage occurring in generation mode.

So we can divide the speed range the generator into 3 parts: the first speed part is between the base speed ω_b and $(2/\sqrt{3})\omega_b$, in this mode the same phases are in series; the second speed part is between $(2/\sqrt{3})\omega_b$ and $2\omega_b$, the adjacent anti-phases are in series; the third speed part is beyond $2\omega_b$, the adjacent phases are in series, the conventional flux weakening control can be further employed to adjust the output voltage for fine tuning. Thus we can switch the different connection mode to the corresponding speed range of the generator in a wide speed range for the constant output voltage. In the starter mode, in order to provide the highest starting torque, connection of same phases in series is chose to meet the requirement of ISG. The generation and starting performance of ISG with single-layer windings and double-layer windings can be analyzed with TS-FEM.

D. Analysis Approach

The TS-FEM is proved to be an effective method to analyze the characteristics of the PM machine [11-14] and now employed to the proposed ISG. The governing equation for electromagnetic field analysis is given by:

$$\frac{\partial}{\partial x}\left(\upsilon\frac{\partial A}{\partial x}\right)+\frac{\partial}{\partial y}\left(\upsilon\frac{\partial A}{\partial y}\right)=-J+\sigma\frac{\partial A}{\partial t}-\upsilon\frac{\partial B_{ry}}{\partial x}+\upsilon\frac{\partial B_{rx}}{\partial y} \tag{1}$$

where A is the magnetic vector potential of the z axis component, υ is the reluctivity, J is the current density, σ is electrical conductivity, it will be exist in the solid rotor iron core and PM where eddy currents cannot be ignored, and B_{rx} and B_{ry} are the remanent flux density vector of the PM in x axis component and y axis component, respectively.

The circuit equation is given by:

$$Ri+L_e\frac{di}{dt}+\frac{l}{S}\iint_{\Omega}\frac{\partial A}{\partial t}d\Omega=u \tag{2}$$

where R is the resistance per phase winding, L_e the inductance of the end windings, i the phase current, l the axial length of iron core, S the conductor area of each turn of phase winding, and Ω the total cross-sectional area of conductors of each phase winding. Then the Galerkin's method is used to derive the system matrix equations as given by:

$$[k]\begin{bmatrix}A\\ i\end{bmatrix}+[k']\begin{bmatrix}\frac{\partial A}{\partial t}\\ \frac{di}{dt}\end{bmatrix}=[p] \tag{3}$$

where $[k]$ and $[k']$ are $(n+m)\times(n+m)$ coefficient matrices, n is the element node number, m is the phase number, $[A]$ and $[i]$ are the value unknown and $[p]$ is the vector value associated with the voltage applied to the stator windings.

The motion equation is given by:

$$J_m\frac{d\omega}{dt}+\alpha_f\omega=T_e-T_f \tag{4}$$

where J_m is the moment of inertia, ω is the rotor speed, T_e is the electromagnetic torque, T_f is the load torque, and α_f is the coefficient of friction. Based on the position of the machine and the conduction current, the transient performance of the ISG is analyzed.

III. RESULTS

By using the circuit-field-torque coupled time-stepping finite-element method (TS-FEM) the magnetic field distribution of the proposed machine can be analyzed. Fig. 7 shows the finite-element mesh and the corresponding magnetic field distribution at full load, in which the iron core magnetic saturation, the eddy-current effect, and the armature reaction are all taken into account. The full load starting performance of both the single-layer and double-layer winding of the proposed ISG in starter mode can be analyzed. Fig. 8 shows the starting performance with single-layer winding and Fig. 9 with double-layer winding. It can be seen that both winding arrangement can meet the requirement that the starting torque is nearly four times the rated torque. The starting torque with double-layer winding is a little higher than with single-layer winding. The reason is that the single-layer winding has more concentrated winding distributions than double-layer winding distribution, which causes greater local armature reaction. However, due to the higher self-inductance and lower mutual inductance with the single-layer winding, which offers improved controllability for ISG application, the single-layer winding structure is chosen for experimentation

For experimental verification, the proposed machine is prototyped as shown in Fig. 10. The specifications of proposed machine is shown in Table I. Fig. 11, Fig. 12 and Fig. 13 show the simulated current waveforms resulted from the TS-FEM and the measured one with the single inner stator, single outer stator and both stators, respectively. Fig. 14 shows the phase current waveform from the TS-FEM and the measured one. As expected, the agreement is very good.

IV. CONCLUSIONS

In this paper a new permanent magnet double-stator ISG has been proposed and implemented for HEVs application. In starter mode, the proposed ISG can achieve a high starting torque for cold cranking. In generation mode, owing to the structure of double-stator windings, a flexible winding connection method can be applied to achieve a constant output voltage over a wide speed range for battery charging. Hence, the proposed ISG is very suitable for the mild HEVs. The simulation results and experimental results confirm the validity of the proposed machine.

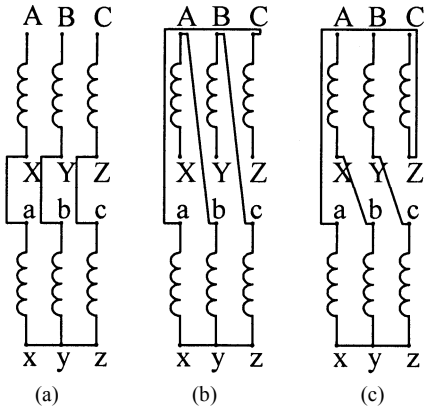

Figure 5. Different connection modes. (a) Same phases in series. (b) Adjacent anti-phases in series. (c) Adjacent phases in series.

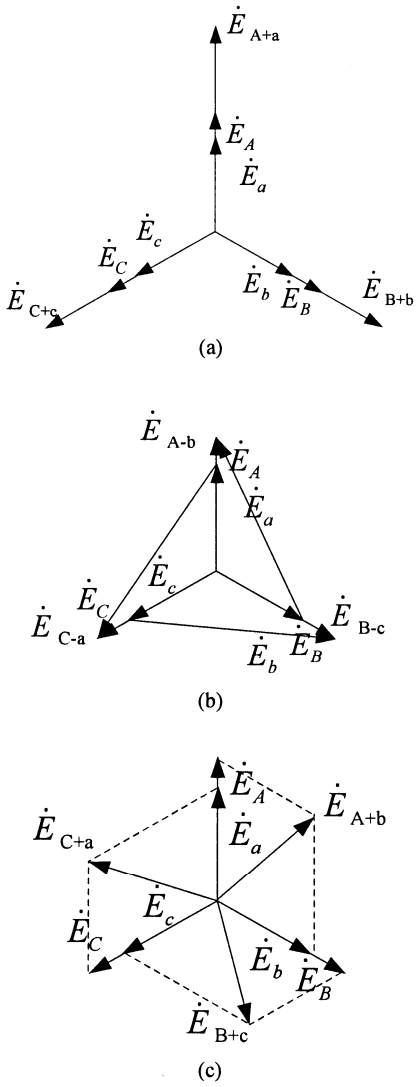

Figure 6. Vector diagrams of different winding connections modes. (a) Same phases in series. (b) Adjacent anti-phases in series. (c) Adjacent phases in series.

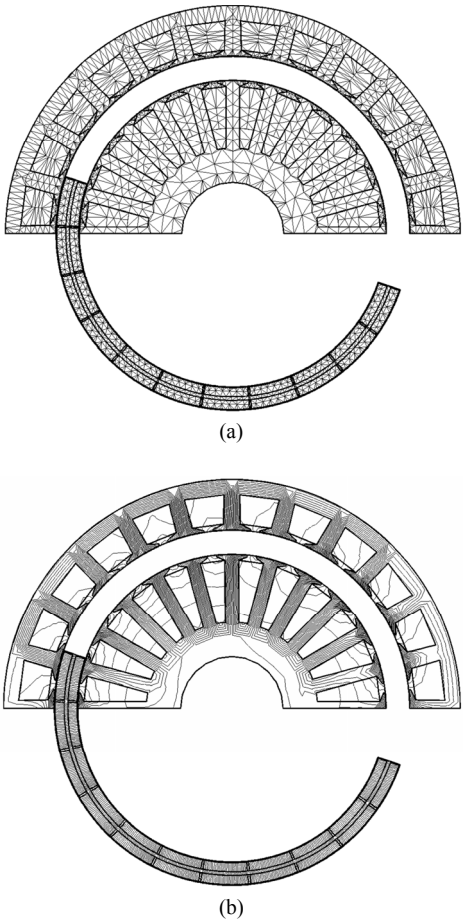

Figure 7. Magnetic field analysis using TS-FEM. (a) Mesh diagram. (b) Magnetic field distribution at full load.

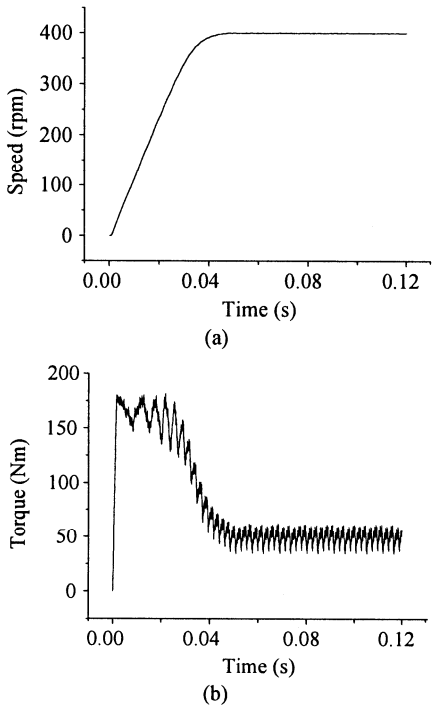

Figure 8. Full-load starting performance with single-layer winding. (a) Speed. (b) Torque.

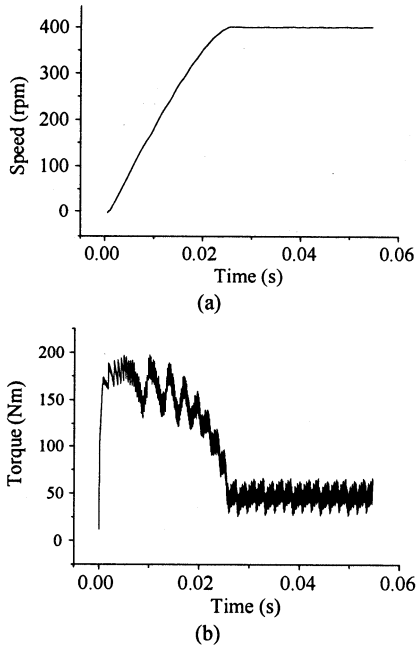

Figure 9. Full-load starting performance with double-layer winding. (a) Speed. (b) Torque.

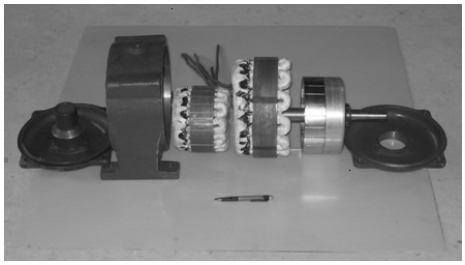

Figure 10. Machine prototype.

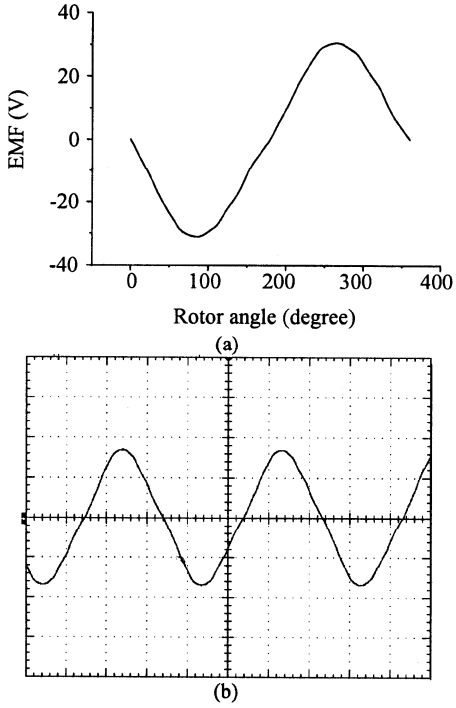

Figure 11. No-load EMF waveforms with inner stator at generation mode. (a) Simulated. (b) Measured (4 ms/div, 20 V/div).

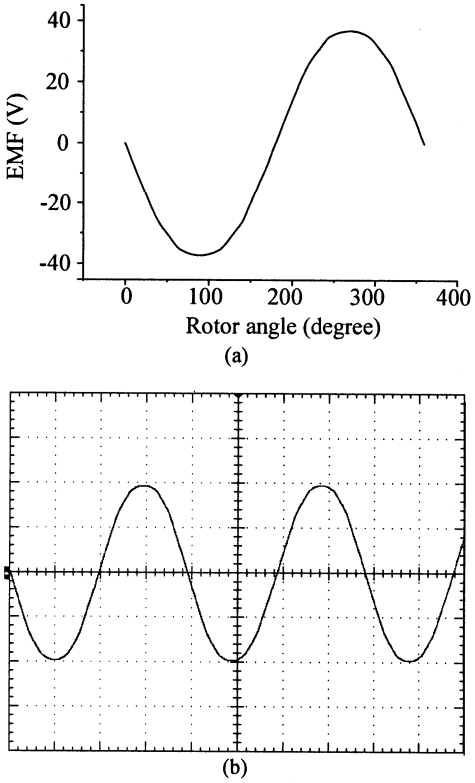

Figure 12. No-load EMF waveforms with outer stator at generation mode. (a) Simulated. (b) Measured (4 ms/div, 20 V/div).

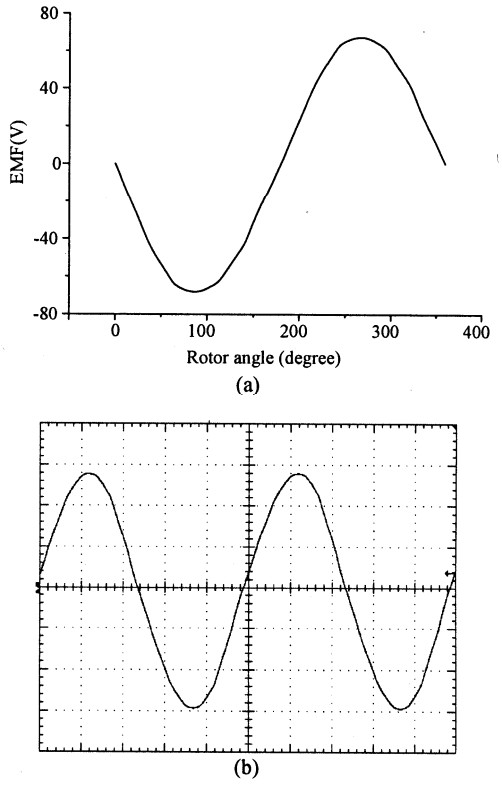

Figure 13. No-load EMF waveforms with outer stator at generation mode. (a) Simulated. (b) Measured (4 ms/div, 20 V/div).

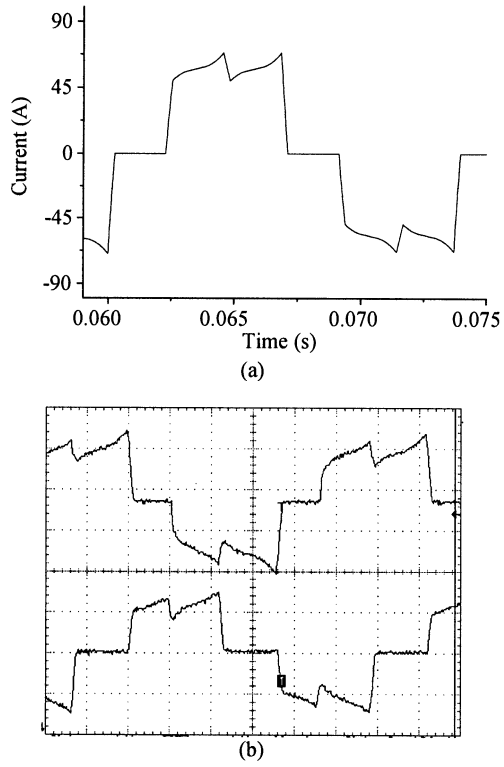

Figure 14. Full-load phase current waveforms at starter mode. (a) Simulated. (b) Measured (2.5 ms/div, 50 A/div).

TABLE I.
SPECIFICATIONS OF PROPOSED MACHINE

Rated speed	400 rpm
Rated power	2 kW
Rated phase voltage	48 V
Inner stator inner diameter	92 mm
Inner stator outer diameter	165 mm
Outer stator inner diameter	191 mm
Outer stator outer diameter	245 mm
Stack length	50 mm
Airgap length	0.6 mm
Inner stator slot number	24
Outer stator slot number	24
Pole number	22

ACKNOWLEDGMENT

This work was supported and funded by a grant (HKU7114/06E) from the Research Grants Council, Hong Kong Special Administrative Region, China.

REFERENCES

[1] C.C. Chan and K.T. Chau, *Modern Electric Vehicle Technology*, Oxford University Press, 2001.

[2] H. Rehman, X. Xu; N. Liu, G.S. Kahlon and R.J. Mohan, "Induction motor drive system for the Visteon Integrated Starter-Alternator"; *The 25th Annual Conference of the IEEE Industrial Electronics Society*, San Jose, CA, USA, vol.2, 1999, pp. 636-641.

[3] C. P. Mudannayake and M. F. Rahman, "An integrated starter alternator for the 42 V PowerNet", *The Fifth International Conference on Power Electronics and Drive Systems (PEDS)*, vol. 1, 2003, pp. 648-653.

[4] A. Walker, P. Anpalahan, P. Coles, M. Lamperth and D. Rodgert, "Automotive integrated starter generator", *The Second International Conference on Power Electronics, Machines and Drives*, vol.1, 2004, pp. 46-48.

[5] A. de Vries, Y. Bonnassieux; M. Gabsi, F. d'Oliveira, and C. Plasse, "A switched reluctance machine for a car starter-alternator system", *IEEE International Electric Machines and Drives Conference, (IEMDC 2001)*, 2001, pp. 323-328.

[6] W. Cai, "Comparison and review of electric machines for integrated starter alternator applications," *IEEE IAS Annual Meeting*, vol. 1, 2004, pp. 386–393.

[7] K.T. Chau, D. Zhang, J.Z. Jiang, C. Liu and Y. Zhang, "Design of a magnetic-geared outer-rotor permanent-magnet brushless motor for electric vehicles," *IEEE Transactions on Magnetics (TM),* Vol. 43, No. 6, June 2007, pp. 2504-2506.

[8] C. Yu, K.T. Chau, X. Liu and J.Z. Jiang, "A flux-mnemonic permanent magnet brushless motor for electric vehicles," *AIP Journal of Applied Physics (JAP)*, Vol. 103, No. 7, January 2008, Paper No. 07F103, pp.1-3.

[9] X. Zhu, K.T. Chau, M. Cheng and C. Yu, "Design and control of a flux-controllable stator-permanent magnet brushless motor drive," *AIP Journal of Applied Physics (JAP)*, Vol. 103, No. 7, April 2008, Paper No. 07F134, pp. 1-3.

[10] S. Niu, K.T. Chau and J.Z. Jiang, "Design and Control of a New Double-Stator Cup-Rotor Permanent-Magnet Machine for Wind Power Generation," *IEEE transaction on magnetics,* vol. 43, no. 6, pp. 2501-2503, 2007.

[11] Y. Wang, K.T. Chau, C.C. Chen and J.Z. Jiang, "Transient analysis of a new outer-rotor permanent-magnet brushless dc drive using circuit-field-torque time-stepping finite element method," *IEEE Trans. on Magnetics*, vol. 38, no. 2, pp. 1297–1300, 2002.

[12] S. J. Salon, *Finite Element Analysis of Electrical Machines,* Norwell, MA: Kluwer, 1995.

[13] Caricchi, F.; Crescimbini, F.; Santini, E.; Santucci, C., "FEM evaluation of performance of axial flux slotted permanent magnet machines," *IEEE Thirty-Third IAS Annual Meeting,* Oct. 1998, vol. 1, pp. 12-17.

[14] K.T. Chau, D. Zhang, J.Z. Jiang and L. Jian, "Transient analysis of coaxial magnetic gears using finite element comodeling," *AIP Journal of Applied Physics (JAP)*, Vol. 103, No. 7, January 2008, Paper No. 07F101, pp.1-3.